Originally published 17 October 2008; corrected 30 October 2008

www.sciencemag.org/cgi/content/full/322/5900/438/DC1

Supporting Online Material for

Surface Sites for Engineering Allosteric Control in Proteins

Jeeyeon Lee, Madhusudan Natarajan, Vishal C. Nashine, Michael Socolich, Tina Vo, William P. Russ, Stephen J. Benkovic, Rama Ranganathan*

*To whom correspondence should be addressed. E-mail: rama.ranganathan@utsouthwestern.edu

Published 17 October 2008, *Science* **322**, 438 (2008)
DOI: 10.1126/science.1159052

This PDF file includes:

CORRECTION (30 October 2008): The originally posted supplement was missing Figure S6.

Supplementary Information

I. Materials and Methods

Multiple Sequence Alignment

Multiple Sequence Alignments (MSAs) of PAS domains and DHFRs, were assembled using PSI-BLAST (*1, 2*) and manually adjusted based on a structural alignment generated using Cn3d (http://www.ncbi.nlm.nih.gov/Structure/CN3D/cn3d.shtml). This resulted in alignments of 1104 PAS domain sequences and 418 DHFR sequences. The alignments of 240 PDZ domains and 717 G-proteins were described by Lockless and Ranganathan (*3*) and Hatley et al.(*4*), respectively.

Statistical Coupling Analysis

Statistical coupling analysis was performed using a custom-written toolbox for MATLAB (SCA Toolbox 2.0); all codes are available upon request from the Ranganathan laboratory. This implementation of SCA represents an updated version of previously published methods (*3, 5*). Briefly, the conservation of an amino acid *a* at position *i* in a multiple sequence alignment taken independently is computed as the relative entropy $D_i^{(a)}$ of the observed frequency $f_i^{(a)}$ at that position at from the average frequency of *a* in all proteins $q^{(a)}$:

$$D_i^{(a)} \approx -\frac{1}{M}\ln P_i^{(a)} = \ln\left[\frac{M!}{(f_i^{(a)}M)!(M-f_i^{(a)}M)!}\left(q^{(a)}\right)^{f_i^{(a)}M}(1-q^{(a)})^{(M-f_i^{(a)}M)}\right],$$

where M the number of sequences in the MSA and $\approx$ represents asymptotical equivalence for large M. The value of $D_i^{(a)}$ quantitatively defines the conservation of amino acids at sites taken independently. The correlation between a pair of amino acids a and b at a pair of positions i and j is defined as the correlation between their site-independent conservations $D_i^{(a)}$ and $D_j^{(b)}$. This is measured through a bootstrap analysis on the MSA in which fluctuations in $D_i^{(a)}$ and $D_j^{(b)}$ are introduced by leaving out each sequence one at a time. Using the notation $D_i^{(a)}(s)$ for the site-independent conservation of amino acid *a* at position *i* in the alignment where sequence *s* is left out, the mean value of $D_i^{(a)}(s)$ over the *M* sequences is denoted $\left\langle D_i^{(a)}(s)\right\rangle_s$. We then define a correlation matrix by:

$$\hat{C}_{ij}^{(ab)} = \left\langle D_{i,s}^{(a)} D_{j,s}^{(b)}\right\rangle - \left\langle D_{i,s}^{(a)}\right\rangle_s \left\langle D_{j,s}^{(b)}\right\rangle_s$$

This measure represents the covariation between a pair of amino acids weighted by the mean fluctuations in their positional conservations– a measure of conserved correlation. For cluster analysis, we reduce the four-dimensional tensor $\hat{C}_{ij}^{(ab)}$ to a two dimensional matrix of positional correlation:

$$\hat{C}_{ij} = \left(\sum_{a,b}\left(\hat{C}_{ij}^{(ab)}\right)^2\right)^{1/2}$$

This updated approach to SCA is more completely discussed in upcoming publications (N. Halabi, O. Rivoire, S. Leibler, and R. Ranganathan, manuscript submitted, and W. Russ, R. Sharma, and R. Ranganathan, manuscript in preparation). Hierarchical clustering was

carried out using modified versions of standard methods in MATLAB using cityblock distances and complete linkage.

Construction of LOV2-DHFR chimeras

E. coli DHFR was cloned as a NcoI/XhoI fragment into the expression vector pHIS8-3, previously described (*6*). Silent mutations were engineered into the DHFR gene using Quikchange (Stratagene) to create unique restriction sites flanking Group A (HindIII beginning at nucleotide 325 of the DHFR gene, and an existing EcoRI site beginning at nucleotide 415) and Group B (MfeI and NotI beginning at nucleotides 242 and 287, respectively) positions. The Quikchange primers are shown in Table S1. Gene fragments encoding the LOV2 domain were cloned between these restriction sites to generate Group A and Group B chimeras, respectively. The LOV2 domain (amino acid residues 404-540) of the *A. sativa* phototropin1 (NPH1-1) [AAC05083], and LOV2 noJ (positions 404-521) were built by the polymerase chain reaction (PCR) using overlapping oligonucleotides (Table S2, AsLOV2_1-AsLOV2_14, or AsLOV2_1-AsLOV2_12 plus AsLOV2_noJ1-AsLOV2_noJ2, respectively) with terminal oligonucleotides that were complimentary to the DHFR sequence and included restriction sites for insertion into Group A or B positions, and amplified using oligos AsLOV2_PF and _PR (Table S2). Dark-locked mutants (C450S) were synthesized similarly by replacing one oligonucleotide containing the mutation (Table S2, AsLOV2_5 replaced with AsLOV2_C450S). Plasmids encoding the chimeric proteins were created by ligation into the Group A or B restriction sites of DHFR. All constructs were verified by DNA sequencing.

Protein Expression and Purification

DHFR-LOV2 chimeric proteins were expressed in BL21 (DE3) cells grown at 37 ºC in Terrific broth to an absorbance at 600 nm of ~1.2 and induced with 0.25 mM IPTG at 18 ºC overnight. Cell pellets were lysed by sonication in binding buffer (0.5 M NaCl, 10 mM imidazole, 50 mM Tris-HCl, pH 8.0) followed by centrifugation and incubation with Ni^{+}-NTA resin (Qiagen) for 30 min at 4 ºC. After washing three times with binding buffer (50 ml/wash) DHFR-LOV2 protein was eluted with elution buffer (1 M NaCl, 400 mM imidazole, 100 mM Tris-HCl, pH 8.0). Eluted protein was dialyzed into dialysis buffer (300 mM NaCl, 1% glycerol/ 50 mM Tris-HCl, pH 8.0) at 4 ºC prior to purification by size exclusion chromatography. Purified protein was concentrated and flash frozen using liquid N_2 prior to enzymatic assays.

Auxotrophic screen

E.coli strain *ER2566* was modified to have a deletion of the DHFR gene (*ER2566 ΔfolΔthy)* and was used for the *in vivo* screen (*7*). The minimal media used in the auxotrophic screen was prepared as described previously (*8*). In the minimal media, the source of purine and other amino acids was limited, and only cells with DHFR activity obtained from the plasmid will survive.

Specific activity of lysate

PAS-DHFR chimera constructs transformed into DHFR mutant strain (ER2566 *ΔthyΔfol*) were grown at 37 ºC in 50 mL of LB containing 50 μg/ml kanamycin and 50

μg/ml thymidine to an absorbance of ~0.6 at 600 nm and then induced at 18 ºC overnight with 200 μM isopropyl β-thiogalactoside. The cells were harvested by centrifugation and the cell pellets were resuspended in 1mL of 25 mM Tris-HCl pH 7.2 with 2 mM DTT and 10% glycerol. Cells were lysed by sonication and insoluble materials were removed by centrifugation. The clear lysate was assayed on a Cary 100 BioUV-Vis spectrophotometer (Varian Inc.) at 25 ºC (*8*). The lysate was preincubated with 100 μM NADPH for 3 min in MTEN buffer at pH 7.0 (50 mM MES [2-(N-morpholino)ethanesulfonic acid], 25 mM Tris [tris(hydroxymethyl)aminomethane], 25 mM ethanolamine, and 100 mM NaCl) containing 2mM DTT, and the reaction was initiated by adding 100 μM dihydrofolate. The decrease in absorbance was monitored at 340 nm ($\Delta\varepsilon_{340}$ =13.2 mM^{-1} cm^{-1})

UV spectral assay

A 2 μl solution of chimeras (~1000 μM), in MTEN buffer pH 7 (*9*), at 25 ºC was scanned in a 2048-element linear silicon CCD array nanodrop spectrometer (ND-1000) under both light and dark conditions. The light was furnished by a 26 W fluorescent lamp held adjacent to the sample. The spectra under both conditions were repeated to ensure the reversibility of the switch (*10*).

Pre-steady-state kinetics of k_{hyd}

Pre-steady-state kinetic experiments to measure the hydride transfer rate (k_{hyd}) were performed on a Applied Photophysics stopped-flow spectrometer. For the single turnover

condition, 20 μM of enzyme solution was preincubated with NADPH (200 μM) in one syringe and less than a stoichiometric amount of H_2F (10 μM) in the other syringe and the two were mixed to initiate the enzyme reaction. The UV absorbance change at 340nm was used to monitor the decrease of NADPH as described previously (*11*). For a light activated reaction, a fluorescent lamp was placed in front of the reaction syringes, which were submerged to a depth of 1 inch in the water bath. The syringe solution was illuminated for five minutes before commencing determination of k_L. After measurements of light activated reactions, the remaining solution in the same syringe was shielded with aluminum foil and dark reaction rates (k_D) were measured. The hydride transfer rate ($k_{D\ (C450S)}$) for a chimera carrying a C450S mutation in the LOV domain was obtained similarly.

Measurement of relaxation rate

Protein samples were initially exposed to a light source as described above for five minutes and the rate constants for decay of the light activated state were measured from the kinetic trace obtained at 340nm. The decay was initiated by covering the window with aluminum foil and k_{hyd} measured at various intervals over 15 minutes for the decay of the light activated state. The rate constants at each time point provide a measure of the relaxation rate (k_{decay}). For relaxation of FMN from its photo activated state, the absorbance change at 447nm was monitored to give $k_{decay\ (FMN)}$. (*12*)

Equilibrium Dissociation Constants

The equilibrium dissociation constant was measured by following the intrinsic protein fluorescence quenching as a function of ligand concentration using a Flouromax-2 or a Flouromax-4 (Horiba Jobin Yvon) spectrofluorometer (*13*). All titrations were performed in MTEN buffer at pH 7.0 containing 1 mM DTT. Tryptophan fluorescence was monitored at 340 nm from excitation at 290 nm. The data were corrected for the inner filter effects and fit as before (*13, 14*). In the case of NADPH binding, a fluorescence cuvette was used to avoid the inner filter effect at the required high concentration of the cofactor due to the weak binding of the chimera. The lit state reactions were performed by illuminating the sample with fluorescent lamp before making measurements. The excitation light from the instrument did not affect photoactivation of the chimera.

Transient-State Kinetics of Ligand Binding

Kinetics of ligand binding, involving on- and off-rate measurements were accomplished by following the ligand dependent quenching of intrinsic protein fluorescence. Protein tryptophans were excited at 290 nm and the resulting fluorescence was measured using a 340 nm interference filter. Rapid mixing with ligand generated a transient quenching of the fluorescence. The data were usually fit to a single exponential function to provide the observed rate. Association rate (k_{on}) measurements for H_4F were performed using a relaxation technique. H_4F dissociation rates(k_{off}) were determined accurately by a competition method with methotrexate as the trapping ligand. Typically, 5 μM of enzyme was incubated with 100 μM of H_4F and for the ternary complex, 1 mM of NADPH or NADP+ was included. Concentration of the competing ligand, methotrexate,

was 1 mM. Details of the principles behind these experiments have been discussed earlier (*13*). Light activated state experiments were carried out by illuminating the stopped flow syringe with fluorescent light for 5 minutes before mixing the solutions.

Proteolysis of the LOV2-DHFR chimera

Limited proteolysis experiments were performed in 50 mM sodium phosphate buffer (pH 7.5) containing 100 mM sodium chloride (*15*). AsLov2 and *E. coli* DHFR were used as controls. Chymotrypsin at a final concentration of 40 μg/mL was added to give a total reaction volume of 100 μL. Samples were incubated at room temperature and aliquots removed after 0, 10, 20, and 60 min for SDS-PAGE analysis. Proteolysis on the light activated protein followed 5min illumination of the solution by a fluorescent lamp. Protein concentration in these experiments was 100 μM.

II. Supplementary Figure Legends and Figures

Figures S1-S5 describe the statistical coupling analysis (SCA) for the four protein families discussed in this work –PDZ, G protein, PAS, and DHFR. Figures S1, S2, S4, and S5 describe (1) an overview of the basic structure and mechanism of each protein family, with specific focus on instances of allosteric signaling processes of relevance for this work, and (2) a basic cluster analysis of the SCA correlation matrix $\hat{C}_{ij}$ for an MSA of the family, and (3) the structural interpretation of the residues identified especially with regard to the allosteric process. Partial SCA analyses for the PDZ and G protein families have been reported before (*3, 4*). For all SCA matrices described, we present here only a first-order analysis of the patterns described by the $\hat{C}_{ij}$ matrix; more intricate patterns of statistical interactions between amino acids are clearly evident that may carry more detailed meaning than is of relevance for this study and that will require further work to understand.

Fig. S1. SCA for the PDZ family. A, the PDZ domain approximately comprises a six-stranded β-sandwich with two asymmetrically positioned helices (α1 and α2) (*16*). The peptide-binding pocket is defined by the second beta strand and the α2 helix. Previous work in the Par-6 PDZ domain has identified the α1 helix as comprising an allosteric surface site at which the binding of regulatory molecules (e.g. Cdc42) can regulate the affinity of the binding pocket for cognate peptide ligands (*17*). B, the $\hat{C}_{ij}$ correlation matrix for an alignment of 240 PDZ domains describing the conserved coevolution of all

pairs of positions. The diagonal values are autocorrelations of sequence positions and are related to the position-specific conservation (see methods) of each position. The matrix is hierarchically clustered, an analysis that reveals a subset of moderately conserved sequence positions that show a pattern of mutual co-evolution (enclosed by white box, and indicated by blue bar). As indicated above, this grouping represents a first order analysis meant to broadly characterize residue correlations rather than serve as a detailed exposition of the information content of the correlation matrix. Sequence positions (Par-6 PDZ numbering) are shown to the right, and positions are colored by the scheme introduced in Figure 1; SCA identified positions within 5A of substrate peptide are in yellow, those buried are in blue, and those that are solvent exposed at in red. As in Figure 2, a residues is declared buried is its fractional solvent exposure is <0.1. **C**, SCA identified residues identified comprise a physically contiguous network of amino acids that basically define the ligand binding pocket and extending to a two specific distant surface sites (see Fig. S3), the largest of which comprises the α1 helix. The linkage of the PDZ binding pocket with the α1 helix is consistent with the known allosteric role of this site in regulation of Par-6 function through binding of the cdc42 G protein (*17*). The color scheme is as described above.

Fig. S2. SCA for the G protein family. A, Structure of Cdc42, a member of the guanine nucleotide-binding (G) protein family. G proteins are binary switches that adopt different conformations (and engage in different molecular interactions) depending on the identity of the bound nucleotide (*18*). Exchange of GTP for GDP at the nucleotide binding pocket triggers a large conformational change at a non-local site (switch 2), a primary region

involved in conserved direct interactions with downstream effector molecules in the G protein family (*18*). B, The $\hat{C}_{ij}$ correlation matrix for an alignment of 717 members of the G protein family (*4*). Clustering indicates a group of strongly correlated amino acid positions (white box and blue bar to right). Sequence positions (Cdc42 numbering) are shown to the right, colored as described in the Fig. S1 legend. C, Residues identified comprise a physically contiguous network of amino acids that largely defines the nucleotide binding pocket, the packing interactions between the switch 2 helix and the core of the G protein, and a few amino acids linking the two. The structure shown corresponds to PDB 1NF3 (*17*).

Fig. S3. Identification of the allosteric interaction surface between the Par6 PDZ domain and cdc42. A-B, A surface analysis of the SCA mappings for the PDZ domain (A) and for the G protein (B) mapped on the atomic structures of the Par6 PDZ domain and cdc42. The coordinates used were extracted from the structure of the complex between the two proteins (PDB code 1NF3). For both proteins, the individual panels show successive 90^{o} rotations of the structure, with SCA residues identified and colored as described in Figs. S1-2: substrate interacting (yellow), buried (blue), and solvent exposed (red). The data show that surface exposed SCA residues occur nearly exclusively at the substrate interactions sites of both proteins and at the allosteric interaction site between the two (Fig. 1B). This represents one example from nature that supports the idea that allosteric communication between protein domains might occur through connection of surface-exposed statistically correlated network positions.

Fig. S4. SCA for the PAS domain family. A, The core PAS domain comprises a five-stranded antiparallel β-sheet with two flanking α-helices and contains a deep ligand binding pocket that opens to one side (*19, 20*). In the LOV2 domain, the pocket contains the FMN chromophore, which upon photon absorption forms a transient covalent interaction with a buried cysteine residue (C450) (*15*). This interaction triggers allosteric conformational changes that lead to unbinding of both a short N-terminal helical domain and the long C-terminal Jα helix (*15, 20*). The structure shown corresponds to PDB 2V0U (*20*). B, The SCA correlation matrix $\hat{C}_{ij}$ for an alignment of 1104 PAS domains (see methods). Cluster analysis reveals a subset of moderately conserved sequence positions that show a pattern of mutual co-evolution (enclosed by white box, and indicated by blue bar). Sequence positions (*A. sativa* LOV2 numbering) are shown along the right margin of the matrix, and are colored as described in Fig. S1. C, The cluster comprises a physically connected network of residues that connects the chromophore-binding site to the specific regions known to undergo light-dependent conformational changes – (1) the N-terminal helical domain and the C-terminal Jα helix, and (2) the α3/β4-β5 region (see text). Note that the MSA (and consequently, the correlation matrix) comprises only the PAS core domain, which excludes the N-terminal helix and all but the first few residues of the Jα helix. The surface sites of the network occur primarily at the regions showing light-dependent conformational change (see Fig. 2A and text).

Fig. S5. SCA for the dihydrofolate reductase (DHFR) family. A, As described in the main text, DHFR comprises a central 8-stranded β-sheet (β-strands A-H) and four flanking α-helices (αB, αC, αE, and αF) that make up an active site cleft that positions the substrate and cofactor for the catalytic step – transfer of hydride from NADPH to the H_2F substrate and reduction to H_4F (*21*). Shown are the βF-βG loop (site A) and the αC-βE loop (site B), which contain the surface sites used for insertion of the LOV2 domain. The dynamics of the βF-βG loop are experimentally known to influence the catalytic rate through mechanical couplings within a network of promoting motions ((*21, 22*), and see Fig. 1C). The structure shown corresponds to PDB 1RX2. B, the $\hat{C}_{ij}$ correlation matrix for an alignment of 418 members of the DHFR family. Clustering reveals a specific subset of residues that are mutually correlated (indicated by white box and blue bar to right). Sequence positions (*E. coli* DHFR numbering) are indicated along the right margin of the matrix, colored as in Fig. S1. C, The residues identified comprise a network of amino acids within DHFR that links the substrate and cofactor binding sites with the βF-βG loop. Much of the network either occurs at the active site or within the protein core; the βF-βG loop positions (red) comprises nearly the only non-local surface site showing strong correlated evolution with the active site (see Fig. 2B). Interestingly, this mapping is consistent with experimental and theoretical work establishing a "network of promoting motions" that couples βF-βG loop dynamics (residues 120-122) to hydride transfer through mechanical interactions in the "Met20 loop" (residues 14-15) and Tyr100; the motion of the network that faciltates hydride transfer is schematically indicated by the arrows (*22*).

Fig. S6. Rescue of growth in the DHFR auxotrophic E.coli strain (ER2566*ΔfolΔthy*) under minimal media conditions by all chimeras. *ER2566 ΔfolΔthy* was transformed with chimeric constructs, the wildtype *E. coli* DHFR (WT), or an empty vector (-ve). Serial dilutions ranging from 0.1 to 1e-4 OD600 units (as indicated by the triangle) were plated on minimal medium (*8*) containing 50 ug/ml kanamycin and 50 μM IPTG, followed by incubation at 30 °C for 4 days.

Fig. S7. Absorbance spectra of dark (black curves) and light exposed (red curves) samples of each of the seven LOV2-DHFR chimeric proteins characterized in this work. The spectra are measured in MTEN buffer pH 7, 25 ºC. In each case, the data show a dark state spectrum consistent with a non-covalently bound FMN chromophore (447 nm peak) which switches to the characteristic lit-state spectrum of the photo-activated LOV2 domain (390 nm peak) that contains the covalent thiol-FMN adduct. The spectra match those reported for the isolated LOV domain (*12*).

Fig. S8. Experiments that varied pH and temperature established pH 7 and 17 ºC to be optimal conditions for A120. A, Temperature effect on the difference of light and dark on the enzyme rate. B, The light/dark difference in the enzyme rate at 17 ºC for three different pH values.

Lee et al.
Figure S1

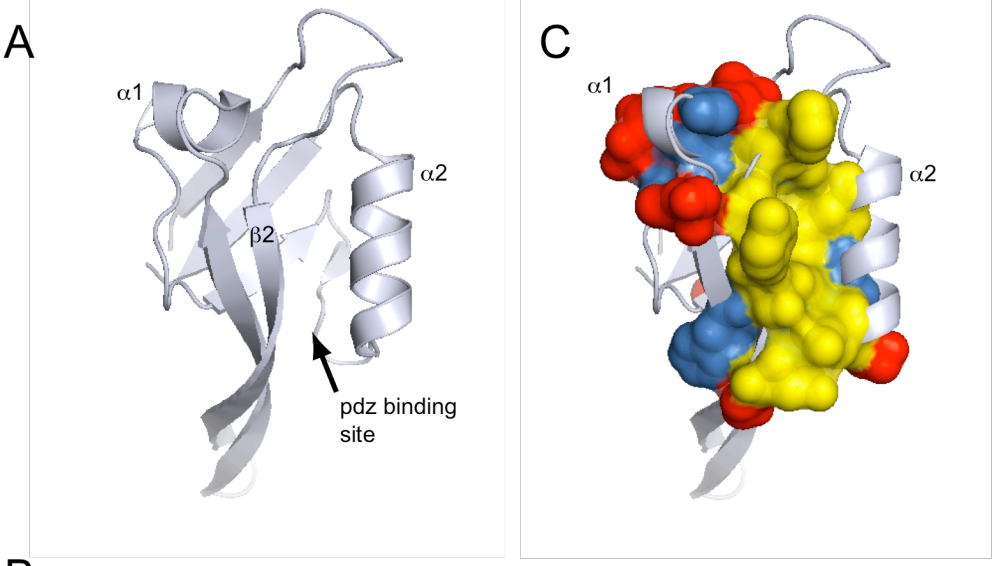

B

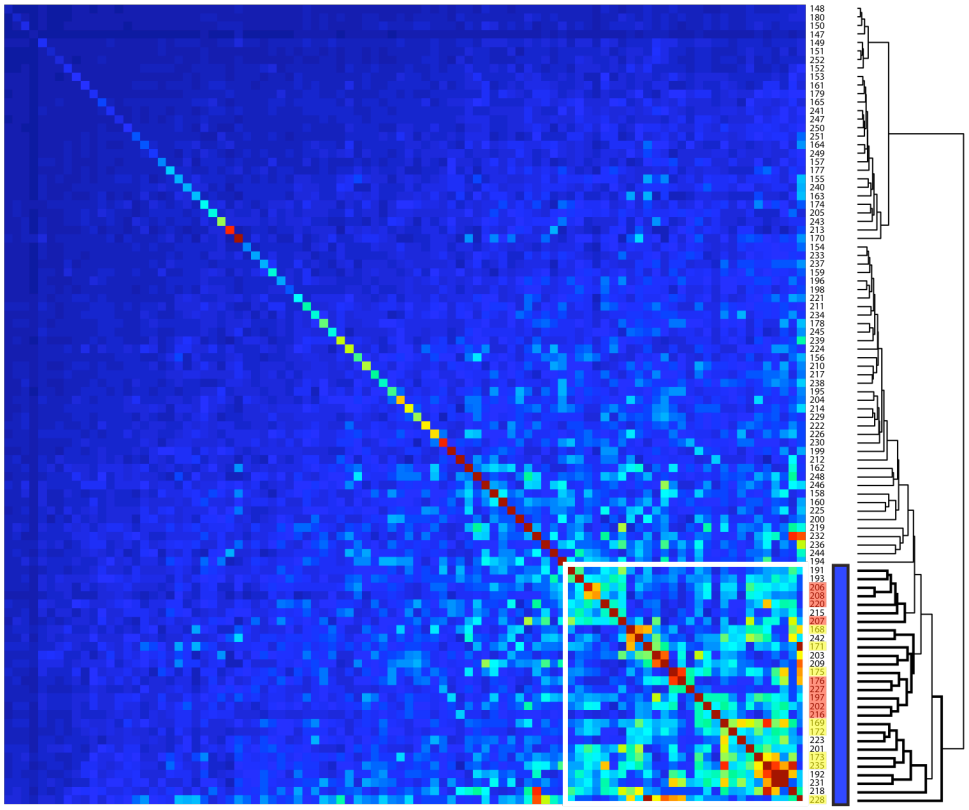

Lee et al.
Figure S2

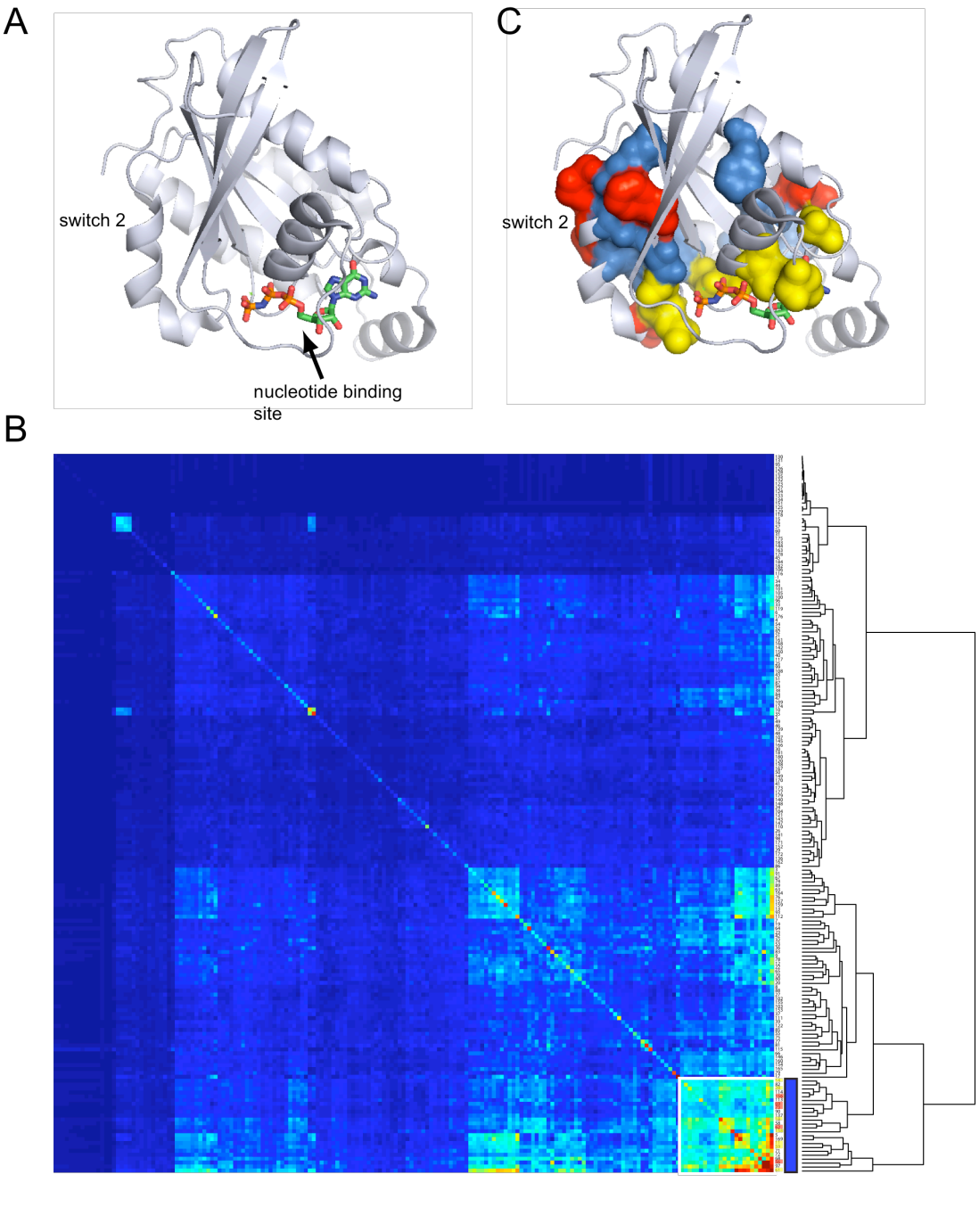

Lee et al.
Figure S3

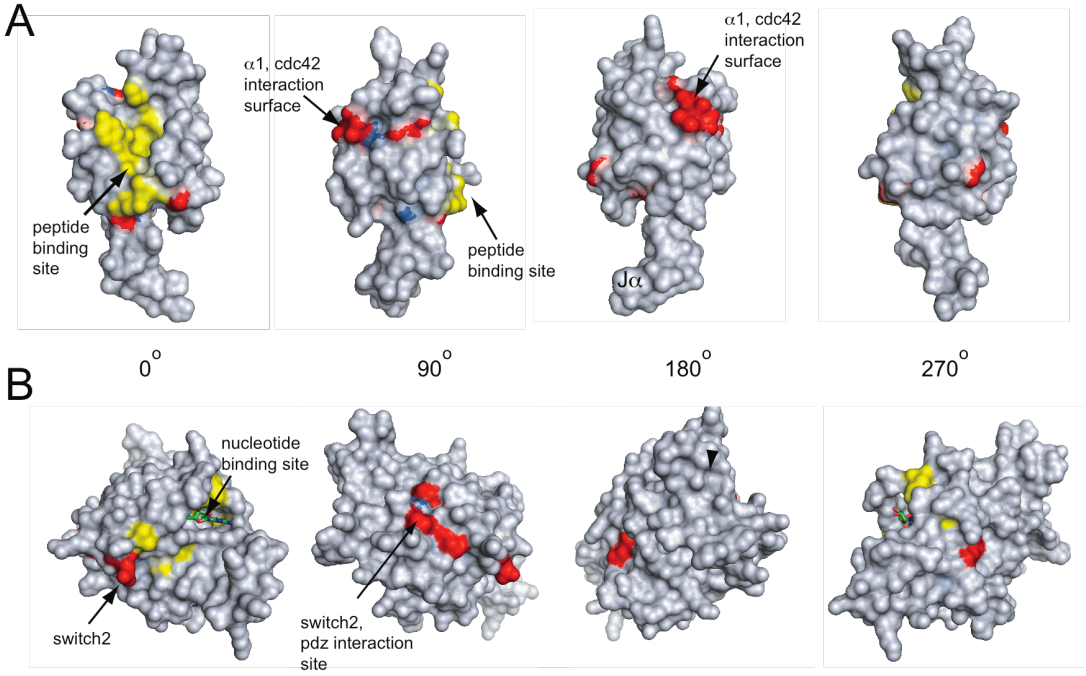

Lee et al.
Figure S4

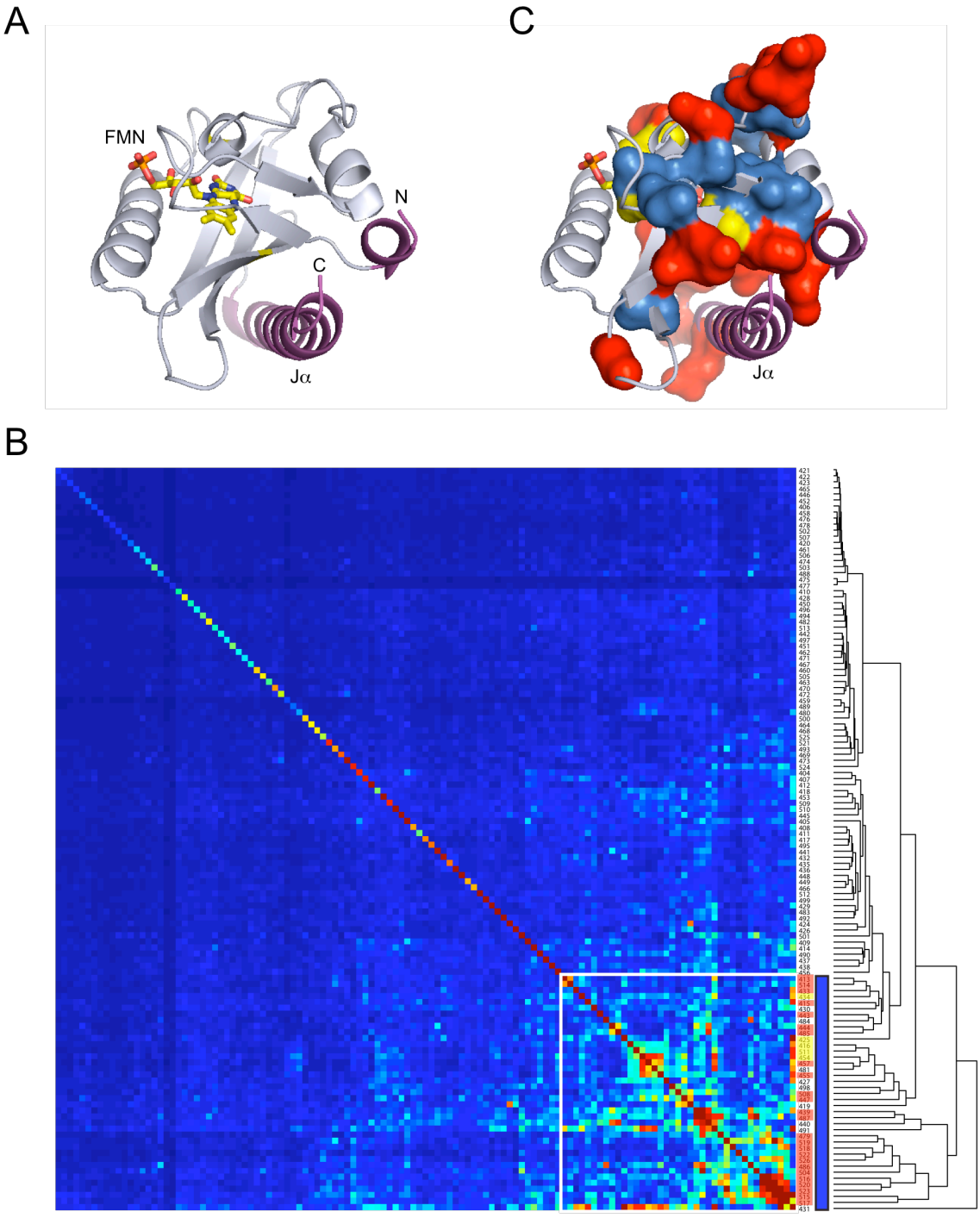

Lee et al.
Figure S5

A

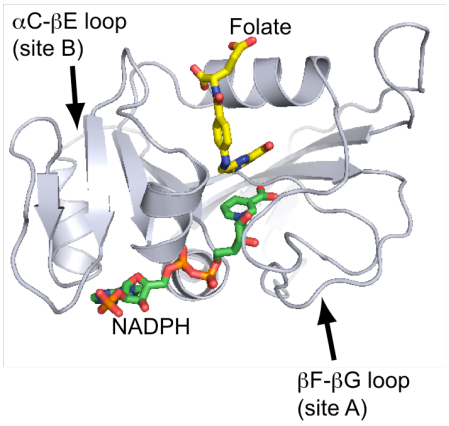

C

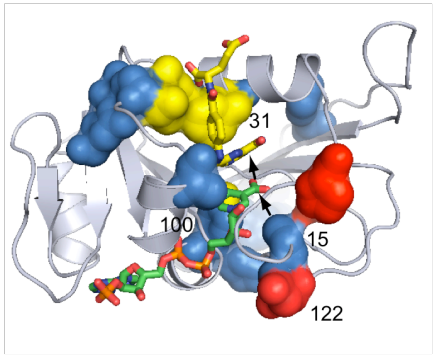

B

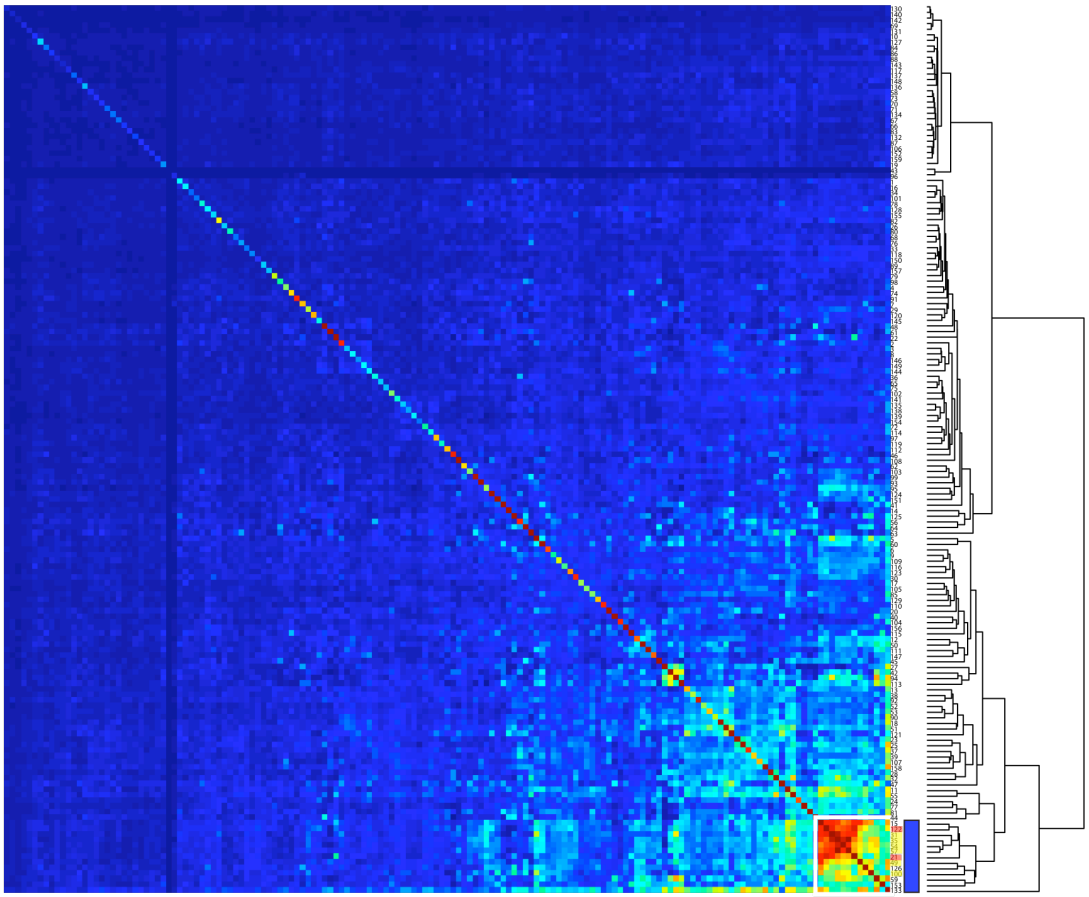

Lee et al.
Figure S6

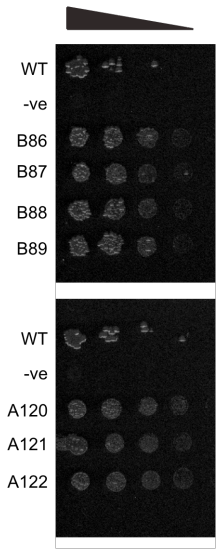

Lee et al.
Figure S7

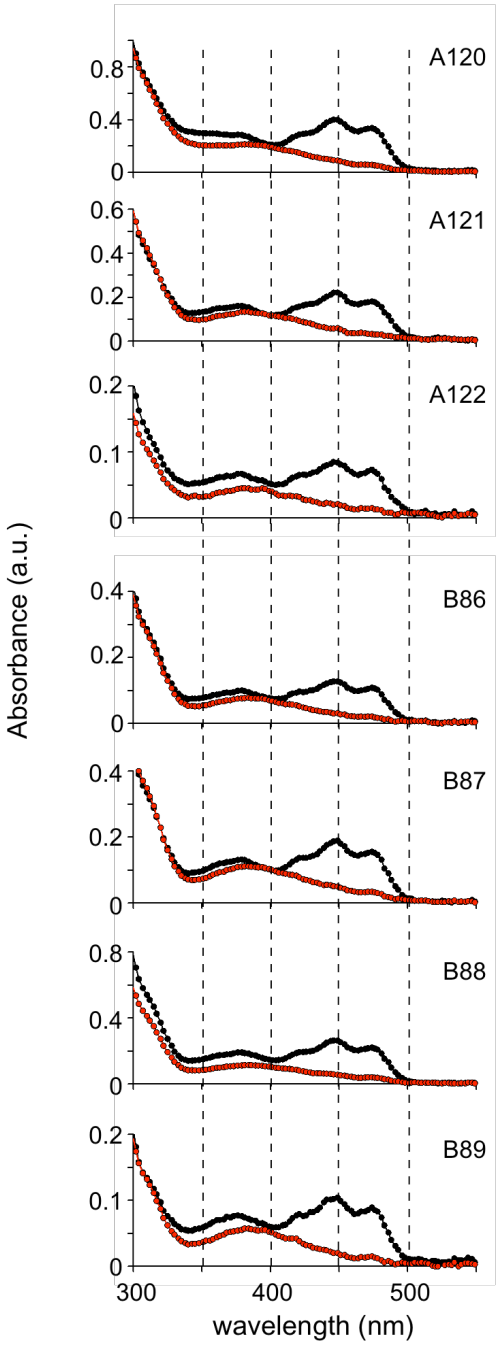

Lee et al.
Figure S8

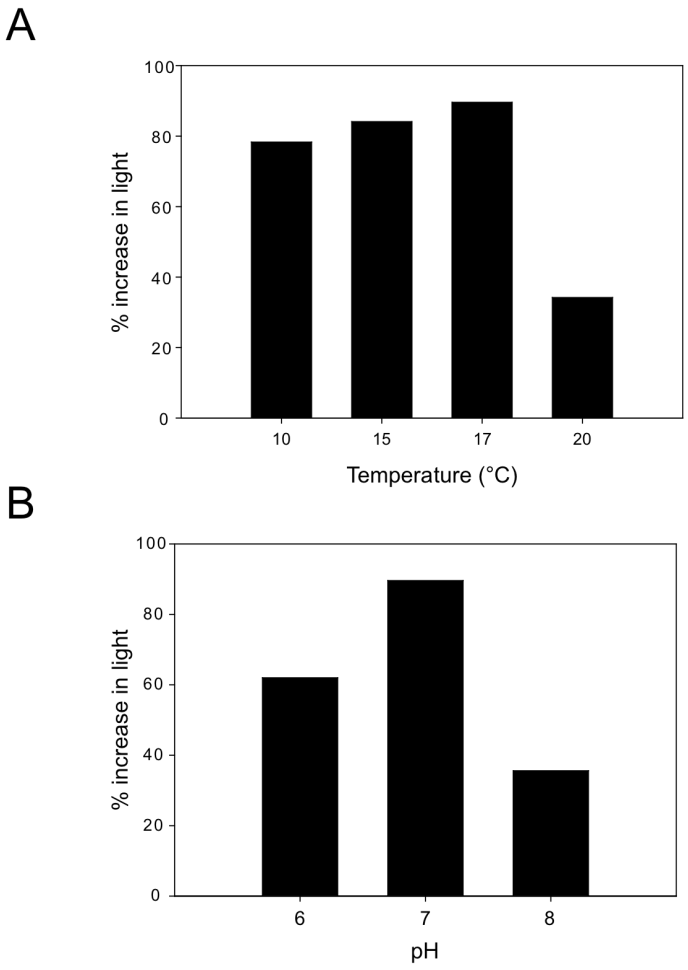

IV. Supplementary Tables

Table S1. Quikchange primers

site	*Primer Name*	*Sequence*
MfeI	g115a_g118t_a	GTCACCACACGCCGCAATTGCTTCATCCACCGAC
	g115a_g118t_b	GTCGGTGGATGAAGCAATTGCGGCGTGTGGTGAC
NotI	a70g_a	CTGTTCATAAACGCGGCCGCCGCCAATCACC
	a70g_b	GGTGATTGGCGGCGGCCGCGTTTATGAACAG
HindIII	c31a_t34c_a	CGTCGATATGCGTCAGATAAAGCTTTTGCGCTTTTGGCAAGA
	c31a_t34c_b	TCTTGCCAAAAGCGCAAAAGCTTTATCTGACGCATATCGACG

Table S2. LOV2 construction oligonucleotides

Name	*Sequence*
AsLOV2_1	CTGGCCACCACTCTAGAGCGCATCGAGAAGAACTTCGTGATCACC
AsLOV2_2	GGGGTTGTCGGGCAGGCGGGGGTCGGTGATCACGAAGTTCTTC
AsLOV2_3	CTGCCCGACAACCCCATCATCTTCGCCTCCGACTCCTTCCTGCAG
AsLOV2_4	GGATCTCCTCGCGGGAGTACTCGGTCAGCTGCAGGAAGGAGTCG
AsLOV2_5	CCCGCGAGGAGATCCTGGGCCGCAACTGCCGCTTCCTGCAGGGCC
AsLOV2_6	CTTGCGCACGGTGGCGCGGTCGGTCTCGGGGCCCTGCAGGAAGC
AsLOV2_7	GCCACCGTGCGCAAGATCCGCGACGCCATCGACAACCAGACCGAG
AsLOV2_8	GGTGTAGTTGATCAGCTGCACGGTCACCTCGGTCTGGTTGTCG
AsLOV2_9	CAGCTGATCAACTACACCAAGTCCGGCAAGAAGTTCTGGAACCTG
AsLOV2_10	GGTCGCGCATGGGCTGCAGGTGGAACAGGTTCCAGAACTTCTTG
AsLOV2_11	CAGCCCATGCGCGACCAGAAGGGCGACGTGCAGTACTTCATCGGC
AsLOV2_12	CACGTGCTCGGTGCCGTCCAGCTGCACGCCGATGAAGTACTGCAC
AsLOV2_13	GGCACCGAGCACGTGCGCGACGCCGCCGAGCGCGAGGGCGTGATG
AsLOV2_14	GTCGATGTTCTCGGCGGTCTTCTTGATCAGCATCACGCCCTCGCG
AsLOV2_15	CGCCGAGAACATCGACGAGGCCGCCAAGGAGCTGCCCGACGCC
AsLOV2_16	GTGGTTGGCCCACAGATCTTCGGGGCGCAGGTTGGCGTCGGGCAGCTC
AsLOV2_noJ1	GGCACCGAGCACGTGCGCGACGCCGCCGAGCGCGAG
AsLOV2_noJ2	GACCGATGCAAGTCTCGAGTTACTCGCGCTCGGCGG
AsLOV2_C450S	CCCGCGAGGAGATCCTGGGCCGCAACTCCCGCTTCCTGCAGGGCC
AsLOV2_PF	CTGGCCACCACTCTAGAGCG
AsLOV2_PR	GTGGTTGGCCCACAGATCTTC

Table S3. Kinetic parameters

T (°C)	*construct*	*trial*	k_D (s^{-1})	k_L (s^{-1})	*% increase in light*
25	A120	1	0.249 ± 0.0012	0.410 ± 0.0015	64.7
		2	0.243 ± 0.0011	0.381 ± 0.0018	56.8
		3	0.246 ± 0.0021	0.393 ± 0.0037	59.8
		mean	**0.246 ± 0.003**	**0.395 ± 0.016**	**60.4 ± 4.0**
	A120-C450S		**0.156 ± 0.0013**	**0.171 ± 0.0039**	**9.6**
17.5	A120		**0.211 ± 0.014**	**0.43 ± 0.018**	**103.8**
	A120-C450S		**0.147 ± 0.018**	**0.164 ± 0.011**	**11.6**

Single turnover experiments were performed at pH 7.0. Errors are reported from at least three trials for each sample.

Table S4: Comparison of the tetrahydrofolate release rates in the lit and the dark states from the E.NH.H_4F ternary complex in MTEN buffer at pH 7.0.

	17.5 ºC			**25.0** ºC		
	$k_{off\ (Lit)}$ (s^{-1})	$k_{off\ (Dark)}$ (s^{-1})	% change	$k_{off\ (Lit)}$ (s^{-1})	$k_{off\ (Dark)}$ (s^{-1})	% change
A120	1.61 ± 0.08	2.05 ± 0.12	1.27	5.85 ± 0.22	4.54 ± 0.36	1.29
A120 C450S	2.08 ± 0.17	2.05 ± 0.10	1.02			

An effect of the light activation was detected in one rate step, $k_{off\ (E.NH.H4F)}$ at (1.29) 25 ºC and (1.27) 17.5 ºC again using sets of data (each set comprising average of 20-25 runs). The data are corrected as before for the decay of the light activated state during the course of the measurement. The value of k_{off} is 12 times faster that the k_{cat} for A120 suggesting that the k_{hyd} step is principally rate limiting.

References:

1. **S. F. Altschul, E. V. Koonin, *Trends in biochemical sciences* 23, 444 (Nov, 1998).**
2. **S. F. Altschul *et al.*, *Nucleic acids research* 25, 3389 (Sep 1, 1997).**
3. **S. W. Lockless, R. Ranganathan, *Science* 286, 295 (Oct 8, 1999).**
4. **M. E. Hatley, S. W. Lockless, S. K. Gibson, A. G. Gilman, R. Ranganathan, *Proc Natl Acad Sci U S A* 100, 14445 (Nov 25, 2003).**
5. **G. M. Suel, S. W. Lockless, M. A. Wall, R. Ranganathan, *Nature structural biology* 10, 59 (Jan, 2003).**
6. **M. Socolich *et al.*, *Nature* 437, 512 (Sep 22, 2005).**
7. **K. A. Datsenko, B. L. Wanner, *Proc Natl Acad Sci U S A* 97, 6640 (Jun 6, 2000).**
8. **M. C. Saraf, A. R. Horswill, S. J. Benkovic, C. D. Maranas, *Proc Natl Acad Sci U S A* 101, 4142 (Mar 23, 2004).**
9. **G. P. Miller, S. J. Benkovic, *Biochemistry* 37, 6336 (May 5, 1998).**
10. **H. Guo, T. Kottke, P. Hegemann, B. Dick, *Biophys J* 89, 402 (Jul, 2005).**
11. **M. H. Penner, C. Frieden, *J Biol Chem* 262, 15908 (Nov 25, 1987).**
12. **M. Salomon, J. M. Christie, E. Knieb, U. Lempert, W. R. Briggs, *Biochemistry* 39, 9401 (Aug 8, 2000).**
13. **C. A. Fierke, K. A. Johnson, S. J. Benkovic, *Biochemistry* 26, 4085 (Jun 30, 1987).**
14. **J. R. Lakowicz, *Principles of fluorescence spectroscopy*. (Springer, ed. 3rd, 2006).**
15. **S. M. Harper, L. C. Neil, K. H. Gardner, *Science* 301, 1541 (Sep 12, 2003).**
16. **D. A. Doyle *et al.*, *Cell* 85, 1067 (Jun 28, 1996).**
17. **S. M. Garrard *et al.*, *The EMBO journal* 22, 1125 (Mar 3, 2003).**
18. **S. R. Sprang, *Annual review of biochemistry* 66, 639 (1997).**
19. **S. Crosson, K. Moffat, *Proc Natl Acad Sci U S A* 98, 2995 (Mar 13, 2001).**
20. **A. S. Halavaty, K. Moffat, *Biochemistry* 46, 14001 (Dec 11, 2007).**
21. **P. T. Rajagopalan, S. J. Benkovic, *Chem Rec* 2, 24 (2002).**
22. **P. K. Agarwal, S. R. Billeter, P. T. Rajagopalan, S. J. Benkovic, S. Hammes-Schiffer, *Proc Natl Acad Sci U S A* 99, 2794 (Mar 5, 2002).**